Stabilizing the C—N Double Bond Character in Fumaramide with the Aid of Superacids

Marie C. Bayer,[a] Nikolaus Greither,[a] Valentin Bockmair,[a] Alexander Nitzer,[a] and Andreas J. Kornath*[a]

Fumaramide was reacted with the superacidic systems XF/SbF_5 and XF/BF_3 (X = H, D) leading to the formation of the O-diprotonated species. Using an equimolar amount of the Lewis acids relating to fumaramide, a mixture of the diprotonated salt and the diadduct with O-coordinated HF was obtained. The salts $[C_4H_2X_6N_2O_2]^{2+}[(BF_4)^-]_2$ and $[C_4H_2X_6N_2O_2]^{2+}[(SbF_6)^-]_2$ (X = H, D) were characterized by low-temperature vibrational spectroscopy. Single-crystal X-ray structure analyses were carried out for the compounds $[C_4H_8N_2O_2]^{2+}[(BF_4)^-]_2$, $C_4H_6N_2O_2\cdots2HF$, and fumaramide. To discuss the experimental results, quantum chemical calculations were executed at the B3LYP/aug-cc-pVTZ level of theory. To investigate the impact of the protonation on the resonance +M effect and the electron distribution concerning the conjugated system ESP maps, NPA charges, and NBO analyses were consulted. Due to the protonation, the nitrogen lone pair contributes completely to the formation of the C=N π-bond, stabilizing the C=N double bond character. Since no monoprotonation of fumaramide is observed, amide hydrolysis is possible simultaneously on both amide groups.

Introduction

The amide bond represents one of the most fundamental functional groups in chemistry and biology.[1] With its remarkable geometrical and energetic features, the amide bond is essential for its structural role as the key facet in the structure of proteins.[2,3] One characteristic of amides is described by the high resonance stabilization, as illustrated by the example of fumaramide in Scheme 1, which is based on the strong influence of the +M effect.[4] As a consequence of amidic resonance, the majority of amides reveal a planar structure.[5-8] The donation from the lone pair on the nitrogen atom into the carbonyl π* orbital results in a 40% double bond character on the C=N bond,[3,4,6,8,9] and a large C=N rotation barrier of around 63–84 kJ mol^{-1}.[3] Hence, the carbon and the nitrogen atoms reveal sp^2 hybridization.[10] The $n_N \rightarrow \pi^*_{C=O}$ conjugation and the concomitant planarity regulate most of the chemical and physical properties of amides.[1,11]

Amide hydrolysis is an essential process in biochemistry occurring via acid catalysis.[12,13] The initial step of amide hydrolysis is the protonation of the amide moiety.[12] The investigation of the protonated amide intermediate helps to gain further information about the reaction mechanism. With two amide groups, fumaramide provides four possible protonation sites serving as interesting starting material for inves-
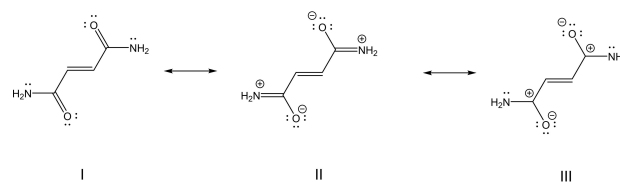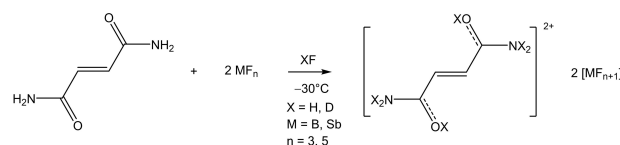

Scheme 1. Resonance structures of fumaramide.

tigations in strongly acidic media. Herein, we present our studies on fumaramide in different binary superacidic systems regarding the protonation site and its impact on amidic resonance.

Results and Discussion

Fumaramide was reacted in the superacidic solutions HF/SbF_5 and HF/BF_3 according to Scheme 2. The O-diprotonated species $[C_4H_8N_2O_2]^{2+}$ was obtained by using an excess of the Lewis acids (SbF_5 or BF_3).

The reactions were performed at a temperature of $-30\,°C$, using anhydrous hydrogen fluoride as solvent as well as a reagent. Subsequently, the excess solvent was removed at $-78\,°C$ in a dynamic vacuum. The salts $[C_4H_8N_2O_2]^{2+}[(BF_4)^-]_2$ (1) and $[C_4H_8N_2O_2]^{2+}[(SbF_6)^-]_2$ (2) were obtained as colorless crystals

[a] M. C. Bayer, N. Greither, V. Bockmair, A. Nitzer, Prof. Dr. A. J. Kornath
Department Chemie
Ludwig-Maximilians-Universität München
Butenandtstr. 5–13(D), 81377 München, Deutschland
E-mail: andreas.kornath@cup.uni-muenchen.de

Scheme 2. Reaction of fumaramide in HF/SbF_5 and in HF/BF_3.

EurJIC
European Journal of Inorganic Chemistry

Research Article
doi.org/10.1002/ejic.202200501

Chemistry Europe
European Chemical
Societies Publishing

and are stable at room temperature. The respective deuterated compounds $[C_4D_6H_2N_2O_2]^{2+}[(SbF_6)^-]_2$ (3) and $[C_4D_6H_2N_2O_2]^{2+}[(BF_4)^-]_2$ (4) were synthesized by modifying the superacid systems to DF/BF_3 and DF/SbF_5, respectively. Deuterium fluoride provokes an H/D-exchange of all acidic protons, which are in the case of fumaramide also the protons of the amino groups. Bearing in mind that fumaramide holds four possible basic centers, including the amino groups, an eight-to-one ratio of the stronger Lewis acid SbF_5[14] was used to prepare a tri- or tetraprotonated cation. However, even an excess of SbF_5 produces the diprotonated species.

For completeness, an equimolar amount of the Lewis acids in reference to fumaramide was applied to form the monoprotonated salt. Surprisingly, a mixture of the diadduct with O-coordinated HF, $C_4H_6N_2O_2 \cdot 2HF$ (5), and the diprotonated species **1** was obtained. In this work, no monoprotonated species were observed.
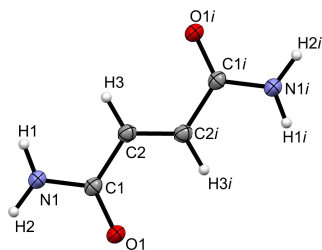

Figure 1. Formula unit of $C_4H_6N_2O_2$ (displacement ellipsoids with 50% probability). Symmetry operation: $i = 1-x, 1-y, 1-z$.

Crystal structure of $C_4H_6N_2O_2$

Since the structural parameters of fumaramide have not been reported yet, we were motivated to investigate the crystal structure. In order to analyze the influence of protonation on the bond lengths and angles, it is important to know the crystal data of the reactant. $C_4H_6N_2O_2$ crystallizes in the monoclinic space group $P2_1/n$ with two formula units per unit cell. The formula unit of fumaramide is shown in Figure 1 and Table 1 summarizes selected structural parameters. The neutral compound exists as the *cis-cis* conformer.

The crystal structure of acetamide[15] is consulted to better compare the crystallographic data of fumaramide. The C1–O1 bond distances of 1.245(2) Å are in agreement with the value 1.247(1) Å found in acetamide[15] and are slightly longer than formal C≡O double bonds (1.19 Å).[16] The C1–N1 bond lengths are with 1.328(2) Å considerably reduced compared to formal C–N single bonds (1.47 Å).[16] They are in accordance with the C–N distance in acetamide (1.335(1) Å).[15] The elongation of the C≡O bond and the simultaneous shortening of the C–N bond demonstrates the importance of the resonance structure II in fumaramide (Scheme 1). With a bond distance of 1.322(2) Å the C2–C2i does not differ from the value for formal C≡C double bonds (1.33 Å).[16] The C1–C2 bond length of 1.487(2) Å is slightly shortened compared with formal C–C single bonds (1.54 Å).[16] The angles found in the molecule deviate up to 4.5° from the ideal bond angle of 120° for sp^2 hybridized carbon atoms. The molecule of fumaramide is found to be almost planar. The variation of the NH_2 groups from the median plane through the molecule amounts to 2.6°.

Table 1. Selected bond lengths and angles of $C_4H_6N_2O_2$ (symmetry operations: $i = 1-x, 1-y, 1-z$; $ii = 2-x, -y, 1-z$; $iii = -0.5+x, 0.5-y, -0.5+z$), $C_4H_6N_2O_2 \cdot 2HF$ (5) (symmetry operations: $i = -x, 1-y, 1-z$; $ii = -1+x, y, 1+z$; $iii = x, 1.5-y, 0.5+z$), and $[C_4H_8N_2O_2]^{2+}[(BF_4)^-]_2$ (1) (symmetry operations: $i = -x, -y, 1-z$; $ii = -1+x, y, z$; $iii = 1-x, 1-y, 1-z$; $iv = -x, 1-y, 1-z$; $v = -1.5+x, 0.5-y, -0.5+z$) with estimated standard deviation marked in parentheses.

Bond length [Å]	$C_4H_6N_2O_2$	$C_4H_6N_2O_2 \cdot 2HF$ (5)		$[C_4H_8N_2O_2]^{2+}[(BF_4)^-]_2$ (1)
C2–C2i	1.322(2)	1.323(2)		1.324(2)
C1–C2	1.487(2)	1.485(2)		1.468(2)
C1–O1	1.245(2)	1.259(2)		1.301(1)
C1–N1	1.328(2)	1.314(2)		1.288(2)
Bond angle [°]				
O1–C1–N1	122.5(1)	122.8(1)		123.8(1)
O1–C1–C2	122.0(1)	120.0(1)		116.4(1)
N1–C1–C2	115.5(1)	117.2(1)		119.8(1)
C1–C2–C2i	122.3(1)	121.0(1)		121.3(1)
Angle of Torsion [°]				
O1–C1–C2–C2i	1.3(2)	5.0(2)		1.9(2)
N1–C1–C2–C2i	−177.4(1)	−174.5(1)		−178.1(1)
C1–C2–C2i–C1i	−180.0(1)	−180.0(1)		−180.0(1)
Donor-acceptor distance [Å]				
N1–H1···O1iii	2.862(2)		O1–H4···F1	2.735(1)
N1–H2···O1ii	2.946(2)		O1–H4···F2ii	3.125(1)
F1–H1···O1		2.414(1)	O1–H4···F2iii	3.032(1)
N1i–H3i···F1ii		2.806(1)	C2–H3···F3v	3.125(2)
N1i–H2i···O1iii		2.992(2)	N1–H2···F2iii	2.976(1)
			N1–H2···F1iv	2.965(1)
			N1–H1···F3v	2.830(1)

EurJIC
European Journal of Inorganic Chemistry

Research Article
doi.org/10.1002/ejic.202200501

**Chemistry
Europe**
European Chemical
Societies Publishing

In the crystal packing of $C_4H_6N_2O_2$, the molecules are connected via two hydrogen bonds which are illustrated in Figure S1 and described in the Supporting Information.

Crystal structure of $C_4H_6N_2O_2 \cdots 2HF$

$C_4H_6N_2O_2 \cdots 2HF$ (5) crystallizes in the monoclinic space group $P2_1/c$ with two formula units per unit cell. Figure 2 shows the formula unit of the diadduct of fumaramide with HF and Table 1 holds selected structural parameters.

The formation of the diadduct of fumaramide with HF leads to a further elongation of the C1–O1 distances of 1.259(2) Å when compared with the starting material. The C1–N1 single bond lengths of 1.314(2) Å are shortened in comparison to fumaramide. In the crystal structure of **5**, fumaramide molecules are linked through two different hydrogen bonds with hydrogen fluoride molecules, as illustrated in Figure S3 and described in the Supporting Information.

Crystal structure of $[C_4H_8N_2O_2]^{2+}[(BF_4)^-]_2$

The diprotonated fumaramide $[C_4H_8N_2O_2]^{2+}[(BF_4)^-]_2$ (1) crystallizes in the monoclinic space group $P2_1/n$ with two formula units per unit cell. Figure 3 shows the formula unit of **1** and corresponding selected bond lengths and angles combined in Table 1.

The diprotonation of fumaramide has a major influence on the C=O bond lengths. In comparison to fumaramide, the C1–O1 bond distances (1.301(1) Å) are significantly elongated by 0.056 Å and slightly shorter than formal C–O single bonds (1.43 Å).[16] The C1–N1 bond lengths of 1.288(2) Å are significantly shorter in contrast to the starting material and are in the range of formal C=N double bonds (1.22 Å).[16] Also, the C1–C2 bond distances of 1.468(2) Å are significantly decreased due to the protonation, compared to the reactant. In comparison with protonated acetamide, the C–O (1.292(3) Å), C–N (1.285(4) Å) and C–C (1.470(4) Å) bond distances are in the same range, respectively.[17] The C2–C2i double bonds are not significantly
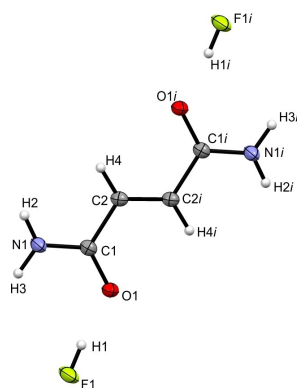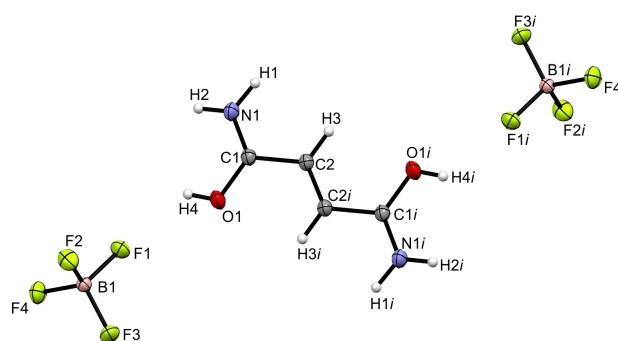

Figure 3. Formula unit of $[C_4H_8N_2O_2]^{2+}[(BF_4)^-]_2$ (displacement ellipsoids with 50% probability). Symmetry operation: $i = -x, -y, 1-z$.

affected by the protonation. As regards bond angles, the greatest impact is observed for the O1–C1–C2 bond angle, which is reduced by 5.6° to 116.4(1)°. The N1–C1–C2 bond angle, on the other hand, is widened by 4.3° to 119.8(1)°, in contrast to fumaramide. The torsion angles in the dication approach the ideal planar values, which means that the OH and the NH$_2$ moieties are twisted out of the carbon plane by merely 1.9°.

The B–F bond lengths of the $[BF_4]^-$ anion are in the range between 1.378(2) Å and 1.403(2) Å. The data are in good accordance with reported B–F bond distances of $[BF_4]^-$ anions.[18] The bond angles in the anion deviate marginally from the ideal tetrahedral bond angle.

In the crystalline state of **1**, the cations and anions are linked via several hydrogen bonds and intermolecular contacts, which are illustrated in Figure S5 and described in the Supporting Information.

Vibrational spectra

The low-temperature vibrational spectra of $[C_4H_8N_2O_2]^{2+}[(BF_4)^-]_2$ (1), $[C_4H_8N_2O_2]^{2+}[(SbF_6)^-]_2$ (2), $[C_4D_6H_2N_2O_2]^{2+}[(SbF_6)^-]_2$ (3), together with fumaramide are displayed in Figure 4. The Raman and corresponding IR spectra of **3** in combination with $[C_4D_6H_2N_2O_2]^{2+}[(BF_4)^-]_2$ (4) and fumaramide are given in Figure S8 in the Supporting Information. Selected experimental vibrational frequencies of **1** and **2** combined with the quantum chemically calculated frequencies of the N-coordinated HF complex of the cation $[C_4H_8N_2O_2 \cdots 2HF]^{2+}$ are summarized in Table 2. All observed frequencies of **1** and **2** are listed in Table S2 and the experimental frequencies of **3** and **4** are summarized in Table S3 in the Supporting Information. To improve the accordance of the calculated frequencies with the experimental ones, two HF molecules were added to the gas phase structure of the cation coordinating the amino group to simulate hydrogen bonds in the solid state.[19] Since the vibrational spectra of fumaramide have not been thoroughly reported yet,[20] we determined the vibrational frequencies of our reactant. To assign the vibrational frequencies of the diprotonated species, the comparison with the neutral com-
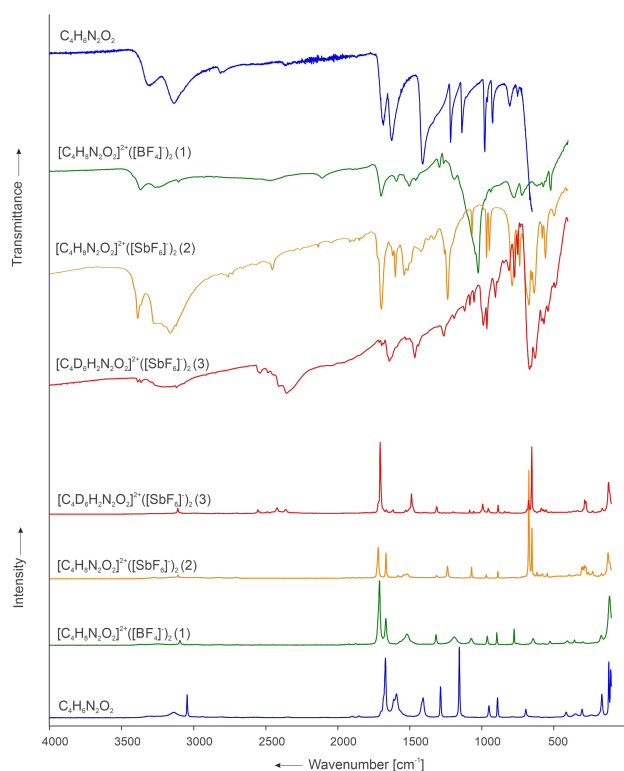

Figure 2. Formula unit of $C_4H_6N_2O_2 \cdots 2HF$ (displacement ellipsoids with 50% probability). Symmetry operation: $i = -x, 1-y, 1-z$.

EurJIC
European Journal of Inorganic Chemistry

Research Article
doi.org/10.1002/ejic.202200501

Chemistry Europe
European Chemical
Societies Publishing

Figure 4. Low-temperature Raman and IR spectra of fumaramide, $[C_4H_8N_2O_2]^{2+}[(BF_4)^-]_2$ (1), $[C_4H_8N_2O_2]^{2+}[(SbF_6)^-]_2$ (2) and $[C_4D_6H_2N_2O_2]^{2+}[(SbF_6)^-]_2$ (3).

pound is fundamental. The *cis-cis* conformer of fumaramide, which exists in the solid state, is expected to have C_{2h} symmetry with 36 fundamental vibrations ($13 A_g + 5 B_g + 6 A_u + 12 B_u$). The rule of mutual exclusion is applicable,[21] concerning the inversion center of the molecule. The vibrational spectra of

fumaramide were assigned by analyzing the Cartesian displacement vectors of the calculated vibrational modes of $C_4H_6N_2O_2$, as well as by comparing them to literature data for the IR spectrum.[20] The observed and assigned frequencies are listed in Table S4 in the Supporting Information. The diprotonated cations reveal *cis-cis* conformers in the crystalline state, as reported in the section above. The *cis-cis*-$[C_4H_8N_2O_2]^{2+}$ is expected to have C_{2h} symmetry with 42 fundamental vibrations ($15 A_g + 6 B_g + 7 A_u + 14 B_u$). On account of the inversion center of the cation, the rule of mutual exclusion applies.[21] The vibrational frequencies were assigned by analyzing the Cartesian displacement vectors of the calculated vibrational modes of $[C_4H_8N_2O_2]^{2+}$, as well as by comparing them to experimental data of fumaramide. The first evidence for a successful protonation is the O–H stretching vibration, which is observed in the IR spectra at 3369 cm^{-1} **1** and at 3367 cm^{-1} **2**. The symmetric O–H stretching modes are not detectable in the Raman spectra, owing to the poor polarizability of the vibration. In the Raman spectra, the O–D stretching vibrations are observable at 2540 cm^{-1} **3** and at 2546 cm^{-1} **4**. The antisymmetric O–D stretching modes are detected at 2538 cm^{-1} **3** and at 2540 cm^{-1} **4** in the IR spectra. The red-shifts of the ν(O–D) are in agreement with the Teller-Redlich rule for a H/D isotopic effect.[21] The antisymmetric NH$_2$ stretching vibrations, observed in the IR spectra at 3265 cm^{-1} **1**, 3275 cm^{-1} **2**, and at 3161 cm^{-1} **2** are red-shifted up to 141 cm^{-1} compared to the neutral compound. In the IR spectra of **3** and **4**, the antisymmetric ND$_2$ stretching modes are detected at 2484 cm^{-1} **3**, 2486 cm^{-1} **4**, and at 2409 cm^{-1} **3**, 2395 cm^{-1} **4**. The observed red-shifts of the ν(N–D) conform to the Teller-Redlich rule.[21] In the Raman spectrum of **1** the symmetric NH$_2$ stretching vibrations, detectable at 3376 cm^{-1} and 3255 cm^{-1}, are blue-shifted by 67 cm^{-1} and 117 cm^{-1}, respectively, in comparison to the starting material. The equivalent NH$_2$ stretching modes of **2** are observed at 3327 cm^{-1} and 3273 cm^{-1} and are blue-shifted by

Table 2. Selected experimental vibrational frequencies [cm^{-1}] of $[C_4H_8N_2O_2]^{2+}[(BF_4)^-]_2$ (1), $[C_4H_8N_2O_2]^{2+}[(SbF_6)^-]_2$ (2) and calculated vibrational frequencies [cm^{-1}] of the N-coordinated HF complex of the cation $[C_4H_8N_2O_2\cdots2HF]^{2+}$.

$[C_4H_8N_2O_2]^{2+}[(BF_4)^-]_2$ (1) exp.[a]		$[C_4H_8N_2O_2]^{2+}[(SbF_6)^-]_2$ (2) exp.[a]		N-coordinated HF complex of the cation $[C_4H_8N_2O_2\cdots2HF]^{2+}$ calc.[b]	Assignment[c]		
IR	Raman	IR	Raman	IR/Raman			
3369 w		3367 vs		3693 (550/0)	ν_{29}	B_u	ν_{as}(O–H)
	3376 (2)		3327 (1)	3557 (0/153)	ν_2	A_g	ν_s(NH$_2$)
3265 w		3275 vs		3556 (438/0)	ν_{30}	B_u	ν_{as}(NH$_2$)
	3255 (2)		3273 (1)	3359 (0/243)	ν_3	A_g	ν_s(NH$_2$)
		3161 vs		3355 (1616/0)	ν_{31}	B_u	ν_{as}(NH$_2$)
3105 w		3121 vs		3200 (27/0)	ν_{32}	B_u	ν_{as}(C–H)
	3095 (7)		3109 (4)	3195 (0/70)	ν_4	A_g	ν_s(C–H)
	1709 (100)		1719 (29)	1741 (0/292)	ν_5	A_g	ν_s(C=N)
1697 m		1697 vs		1726 (647/0)	ν_{33}	B_u	ν_{as}(C=N)
	1666 (42)		1665 (24)	1699 (0/214)	ν_6	A_g	ν(C=C)
1591 w		1599 s		1621 (175/0)	ν_{34}	B_u	ν_{as}(C–O)
			1541 (4)	1601 (0/19)	ν_7	A_g	ν_s(C–O)
1043 vs		1067 w		1104 (1/0)	ν_{38}	B_u	ρ_{as}(NH$_2$)
	1072 (11)		1071 (11)	1104 (0/28)	ν_{11}	A_g	ρ_s(NH$_2$)
	962 (14)		969 (4)	972 (0/10)	ν_{12}	A_g	ν_s(C–C)
937 w		947 m		939 (31/0)	ν_{39}	B_u	ν_{as}(C–C)
777 m		789 s		807 (204/0)	ν_{17}	A_u	ω_{as}(NH$_2$)

[a] Abbreviations for IR intensities: v = very, s = strong, m = medium, w = weak. IR intensities in km/mol; Raman intensities in Å^4/u. Experimental Raman activities are relative to a scale of 1 to 100. [b] Calculated on the B3LYP/aug-cc-pVTZ level of theory. [c] ρ = rocking, ω = wagging.

EurJIC
European Journal of Inorganic Chemistry

Research Article
doi.org/10.1002/ejic.202200501

Chemistry Europe
European Chemical
Societies Publishing

18 cm^{-1} and 135 cm^{-1}, respectively, compared to fumaramide. The antisymmetric C—H stretching vibrations in the IR spectra of **1** (3105 cm^{-1}) and **2** (3121 cm^{-1}) are red-shifted, whereas the symmetric ones observed in the Raman spectra of **1** (3095 cm^{-1}) and **2** (3109 cm^{-1}) are blue-shifted in contrast to the reactant. The protonation of the oxygen atom has a great impact on the C—N bond. The respective C—N stretching vibration is substantially blue-shifted by 287 cm^{-1} in the IR spectra (1697 cm^{-1} **1**, **2**) and by up to 311 cm^{-1} in the Raman spectra (1709 cm^{-1} **1**, 1719 cm^{-1} **2**). This blue-shift indicates a strengthening of the C—N bond due to the protonation, which is also observed in the crystal data of **1**. The C=C stretching mode appears in the Raman spectra at 1666 cm^{-1} **1** and at 1665 cm^{-1} **2**. By comparing to the starting material, the ν(C=C) is blue-shifted by up to 56 cm^{-1}. As a result of the diprotonation, the C=O bonds are weakened and appear in the IR spectra at 1591 cm^{-1} **1** and at 1599 cm^{-1} **2**, and in the Raman spectrum at 1541 cm^{-1} **2**. These vibrations are red-shifted by up to 128 cm^{-1} compared to fumaramide. The weakening of the C=O bond is confirmed by the crystal structure of **1**. A blue-shift of the C—C stretching vibration of up to 78 cm^{-1} compared to the neutral compound is observed in the IR spectra at 937 cm^{-1} **1**, 947 cm^{-1} **2**, and in the Raman spectra at 962 cm^{-1} **1**, 969 cm^{-1} **2**. The crystal structure of **1** supports the strengthening of the C—C single bond because of the protonation. For the [SbF$_6$]$^-$ anion with ideal O_h three Raman lines and two IR bands are anticipated. Indeed a higher number of vibrations is observed in the spectra of **2** and **3**, implying a distortion of the octahedral structure of the anion. The anion [BF$_4$]$^-$ is assigned to the point group T_d and provides four vibrational modes, which are all Raman active and two of which are IR active.[22] The occurrence of more than these expected vibrations is attributed to a lowering of the symmetry of the ion by solid-state effects. This is verified by the crystal structure of **1**.

Quantum chemical calculations

The quantum chemical calculations were performed at the B3LYP/aug-cc-pVTZ level of theory. The comparison of the experimental data with the calculated frequencies and structural parameters of the free cation [C$_4$H$_8$N$_2$O$_2$]$^{2+}$ reveals a discrepancy (Tables S5 and S6). These differences are caused by several hydrogen bonds present in the crystal structure of **1**. To improve the calculation, different hydrogen bonds are simulated by adding HF molecules to the gas phase structure of the free cation.[19] The comparison of the different calculated bond lengths and angles with the experimental structural parameters revealed that the N-coordinated HF complex of the cation [C$_4$H$_8$N$_2$O$_2$···2HF]$^{2+}$ agrees best with the experimental data (Tables S5 and S6). A comparison of the calculated structure of the cation with N-coordinated HF molecules [C$_4$H$_8$N$_2$O$_2$···2HF]$^{2+}$ with the single-crystal X-ray structure of **1** along with bond lengths and angles is illustrated in Figure S9. All of the experimentally obtained bond lengths and angles of the dication are in good agreement with the calculated structure, except for the bond distances N1—C1 and C2—C3, which are

slightly overestimated in the calculation, in contrast to the experimental data. This is attributable to further hydrogen bonds and intermolecular interactions in the solid state of **1**, which are not regarded in the calculation.

To investigate the diprotonated species and the reactant in terms of the conjugated system, electrostatic potential (ESP) maps in conjunction with natural population analysis (NPA) charges were calculated. Figure 5 illustrates the ESP maps combined with NPA charges of fumaramide and [C$_4$H$_8$N$_2$O$_2$]$^{2+}$. In the following, we focus on the ESP map of the free cation [C$_4$H$_8$N$_2$O$_2$]$^{2+}$ since it provides more details concerning the
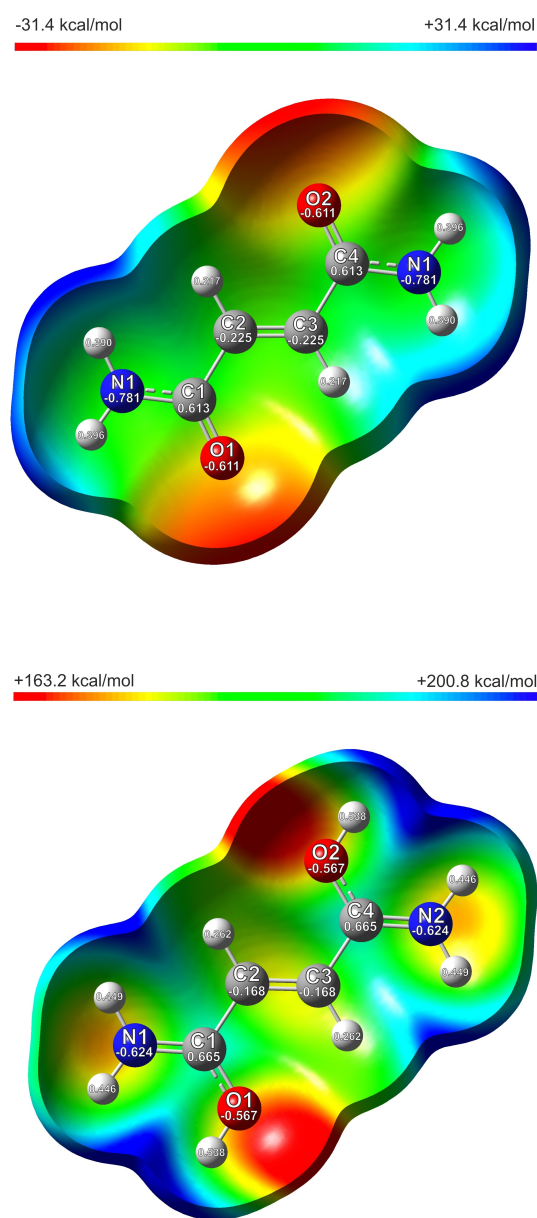

Figure 5. Top: Calculated ESP surface mapped onto an electron density isosurface value of 0.0004 bohr^{-3} with the color scale ranging from −31.4 kcal mol^{-1} to +31.4 kcal mol^{-1} of C$_4$H$_6$N$_2$O$_2$. Bottom: Calculated ESP surface mapped onto an electron density isosurface value of 0.0004 bohr^{-3} with the color scale ranging from +163.2 kcal mol^{-1} to +200.8 kcal mol^{-1} of [C$_4$H$_8$N$_2$O$_2$]$^{2+}$.

EurJIC
European Journal of Inorganic Chemistry

Research Article
doi.org/10.1002/ejic.202200501

Chemistry
Europe
European Chemical
Societies Publishing

conjugated system than the ESP map of the N-coordinated HF complex of the cation $[C_4H_8N_2O_2\cdots2HF]^{2+}$, which is illustrated in Figure S10 in the Supporting Information. The ESP map of fumaramide shows the negative charge density is located in the region around the oxygen atoms displayed by the red surface. The positive electrostatic potential is concentrated in the amino groups. According to the resonance form II in Scheme 1 this charge distribution indicates that the π-electrons are shifted from nitrogen toward oxygen. Both, the σ- as well as the π-electrons are affected by the NPA charge differences between nitrogen and oxygen. The σ-electrons are polarized in the reversed way to the π-electrons.[3] The NPA charges of the nitrogen atoms possess even a higher negative value than the oxygen atoms. The ESP map of the neutral compound shows a neutral electrostatic potential along with the carbon skeleton. The diprotonation of fumaramide entails a realignment of the electrostatic potential distribution, as illustrated in the ESP map of the free cation $[C_4H_8N_2O_2]^{2+}$ in Figure 5 (bottom). The charge density on the amino groups shifted from positive to neutral, whereas the negative charge density, is still concentrated on the carbonyl oxygen atom. A neutral electrostatic potential is also found in the carbon skeleton. The negative NPA charges of the N1 and N2 atoms, as well as of the O1 and O2 atoms decline. It can be assumed that on account of the protonation the electron density of the conjugated system shifts from the oxygen to the nitrogen atoms thereby strengthening the C=N and weakening the C−O bond. The positive electrostatic potential is concentrated in the region between the amino group and the protonated oxygen, displaying the delocalization of the positive charge along the amide moiety. Another positive electrostatic potential is located between the amino group and the CH moiety. Both positive regions indicate exactly where the four-center hydrogen bonds and the bifurcated hydrogen bonds are formed, which is illustrated in Figure 6. The formation
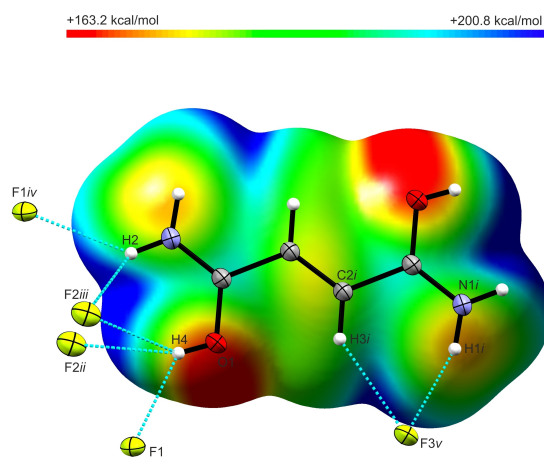
of plenty of hydrogen bonds is favored because the diprotonated fumaramide is highly polar, as illustrated in the ESP map.

To go into further detail, regarding the impact of the diprotonation on the resonance effect and the hybridization, we performed natural bond orbital calculations of $[C_4H_8N_2O_2]^{2+}$ and compared it with fumaramide. The NBO analysis of the neutral compound confirmed that the nitrogen, as well as the carbon atom of the amide moiety, are sp²-hybridized. The nitrogen atom possesses one lone pair, occupied with 1.74 e⁻, which is available for contributing to planar amidic bond resonance ($n_N \rightarrow \pi^*_{C=O}$ conjugation),[5,23] which is illustrated in Figure 7. According to the NBO calculations, the oxygen atom reveals sp-hybridization. The conjugation in fumaramide changes significantly due to the diprotonation. The nitrogen and the carbon atoms are still sp²-hybridized. However, the nitrogen lone pair is not located at the nitrogen anymore. It contributes completely to the formation of the C=N π-bond, as shown in Figure 7. The diprotonation supports the +M effect and thereby favoring the resonance form II (Scheme 1). Simultaneously the resonance form I gets irrelevant for the diprotonated species. The assumption arises that in the diprotonated species the double bond character increases from 40%[6] to 100% and the resonance effect becomes obsolete. On account of the protonation, the C=N double bond character is stabilized. A rehybridization is observed from sp to sp² for the oxygen atom.

We were interested to find out if an additional N-protonation on the amide moiety is theoretically possible. An inspiring example in which an N,O-diprotonation was observed, is represented by urea.[24] Urea can be described as one amide group combined with one amino moiety. The O-monoprotonation is followed by the N,O-diprotonation. However, the additional N-protonation of urea takes place in the amino group and leads to the formation of $-NH_3^+$. Interestingly, the nitrogen atom of the amide moiety remains unprotonated and no triprotonation is found for urea.[24]

Since the nitrogen atoms of the diprotonated fumaramide have no lone pairs at their disposal, a further protonation on the nitrogen atoms leading to tri- and fourfold-protonated species seems to be impossible. Although O-protonation is preferred over N-protonation in simple amides, such as fumaramide, there is evidence for N-protonation appearing to be favored for instance in strained molecular systems.[13] As O-protonated cations become planar, N-protonation provokes disruption of the amide bond resonance.[11,13] We assume that a
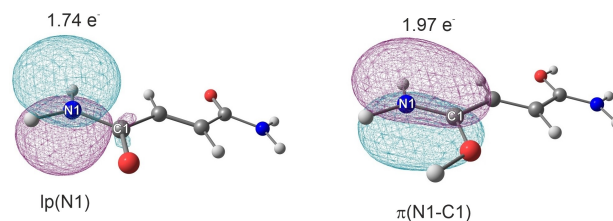

Figure 6. Selected hydrogen bonds in the crystal structure of 1 (displacement ellipsoids with 50% probability). The hydrogen bonds are drawn as dashed blue lines. The calculated ESP surface mapped onto an electron density isosurface value of 0.0004 bohr⁻³ with the color scale ranging from +163.2 kcal mol⁻¹ to +200.8 kcal mol⁻¹. Symmetry operations: $i=-x, -y, 1-z$; $ii=-1+x, y, z$; $iii=1-x, 1-y, 1-z$; $iv=-x, 1-y, 1-z$; $v=1.5-x, -0.5+y, 1.5-z$.

Figure 7. Selected NBOs for the nitrogen lone pair of fumaramide (left) and for the CN bond of $[C_4H_8N_2O_2]^{2+}$ (right) with corresponding occupancies.

EurJIC
European Journal of Inorganic Chemistry

Research Article
doi.org/10.1002/ejic.202200501

Chemistry Europe
European Chemical
Societies Publishing

further N-protonation leads to a distortion of the planarity of the molecular system which comes along with a loss of symmetry and is therefore not observed.

Conclusion

Fumaramide was examined in the superacidic systems XF/SbF_5 and XF/BF_3 (X = H, D). The salts of the O-diprotonated fumaramide were isolated and characterized by low-temperature vibrational spectroscopy. Using an equimolar amount of the Lewis acids in relation to fumaramide, a mixture of the diprotonated salt and the diadduct with O-coordinated HF was obtained. Single-crystal X-ray structure analyses were performed for $[C_4H_8N_2O_2]^{2+}[(BF_4)^-]_2$, $C_4H_6N_2O_2 \cdots 2HF$, as well as for the neutral compound fumaramide. To interpret the experimental results, quantum chemical calculations were executed at the B3LYP/aug-cc-pVTZ level of theory. To investigate the impact of the protonation on the resonance +M effect and the electron distribution concerning the conjugated system ESP maps, NPA charges, and NBO analyses were consulted. On account of the protonation the electron density of the conjugated system shifts from the oxygen atoms to the nitrogen atoms thereby strengthening the C=N and weakening the C–O bond, which is confirmed by crystal data and vibrational frequencies. Owing to the protonation the C=N double bond character is stabilized. Since no monoprotonation of fumaramide is observed, amide hydrolysis is possible simultaneously on both amide groups. Fumaramide is especially suitable for biochemical hydrolysis reactions of both amide moieties.

Experimental Section

Caution! Contact with the components must be avoided. The hydrolysis of SbF_5, BF_3, and the reported salts might release HF, burn skin, and cause irreparable damage. Adequate safety precautions must be undertaken when using and handling these materials.

Apparatus and materials: The reactions were conducted by using standard Schlenk techniques with an electropolished stainless-steel vacuum line. Transparent FEP/PFA-reactors in combination with stainless-steel valves were employed for the reactions in superacidic media. The vacuum line, as well as the reactors, were dried with fluorine, before use. Excess fluorine was removed in a dynamic vacuum and absorbed by Sodalime. Antimony pentafluoride was managed in a Duran glass high vacuum line by using Young valves. Low-temperature Raman spectroscopic measurements were performed in a glass cell under vacuum cooled down to −196 °C on a Bruker MultiRAMII FT-Raman spectrometer with Nd:YAG laser excitation ($\lambda = 1064$ nm). For the IR measurements, the respective sample was put on a CsBr single-crystal plate in a cooled cell. A Bruker Vertex-80 V-FT-IR spectrometer was used for recording the low-temperature IR spectra. The low-temperature single-crystal X-ray diffractions of $C_4H_6N_2O_2$, **1**, and **5** were conducted on an Oxford XCalibur3 diffractometer equipped with a Spellman generator (50 kV, 40 mA) and a Kappa CCD-detector, which operates with MoK_α radiation ($\lambda = 0.71073$ Å). Data collection and reduction were performed using the program CrysAlisPro 1.171.38.46 (Rigaku OD, 2015).[25] The crystal structures were solved using SHELXT[26] and SHELXL-2018/3[27] of the WINGX software package.[28] The structures were checked by applying the software PLATON.[29] The absorption correction was performed with the help of the SCALE3 ABSPACK multiscan method.[30] Selected data and parameters of the reported single-crystal structures $C_4H_6N_2O_2$, **1**, and **5** are summarized in Table S8 (Supporting Information). Quantum chemical calculations were carried out on the B3LYP/aug-cc-pVTZ level of theory using the software package Gaussian 09[31] and Gaussian 16.[32] Gauss-View 6.0 was used for the visualization and illustration of the ESP calculations.[33]

Syntheses of $[C_4H_8N_2O_2]^{2+}[(BF_4)^-]_2$ (1) and $[C_4D_6H_2N_2O_2]^{2+}([BF_4]^-)_2$ (4): At first, boron trifluoride (203 mg, 3.00 mmol) was condensed into an FEP reactor vessel at −196 °C. Approximately 2 mL of anhydrous hydrogen fluoride (aHF) (**1**) or deuterium fluoride (aDF) (**4**), respectively, were condensed into the FEP reactor vessel at −196 °C. The superacid was warmed up to −10 °C, homogenized, and accordingly refreezed at −196 °C. Under a nitrogen atmosphere fumaramide (114 mg, 1.00 mmol) was added to the frozen mixture. The reaction mixture was warmed up to −30 °C and mixed until the solution was clear. In dynamic vacuum excess HF or DF, respectively, was removed at −78 °C. The compounds were obtained as colorless crystalline solids being stable up to 20 °C. The rector was left in an ethanol bath at −40 °C for crystallization of **1**.

Syntheses of $[C_4H_8N_2O_2]^{2+}([SbF_6]^-)_2$ (2) and $[C_4D_6H_2N_2O_2]^{2+}([SbF_6]^-)_2$ (3): Antimony pentafluoride (370 mg, 1.71 mmol) was condensed into an FEP reactor vessel at −196 °C. In addition, approximately 2 mL of anhydrous hydrogen fluoride (aHF) (**2**) or deuterium fluoride (aDF) (**3**), respectively, were condensed into the FEP reactor vessel at −196 °C. The mixture was warmed up to −10 °C, homogenzied and afterwards refreezed at −196 °C. Fumaramide (65 mg, 0.57 mmol) was added under a nitrogen atmosphere to the frozen mixture. The reaction mixture was warmed up to −30 °C and homogenized until the formed salt was dissolved thoroughly. Excess HF or DF, respectively, was removed in a dynamic vacuum at −78 °C. The compounds were obtained as colorless crystalline solids, which are stable up to 20 °C.

Syntheses of $C_4H_6N_2O_2 \cdots 2HF$ (5): At the beginning, boron trifluoride (68 mg, 1.00 mmol) was condensed into an FEP reactor vessel at −196 °C. Approximately 2 mL of anhydrous hydrogen fluoride (aHF) were condensed into the FEP reactor vessel at −196 °C. To form the superacid, the mixture was warmed up to −10 °C, homogenized, and accordingly refreezed at −196 °C. Under a nitrogen atmosphere fumaramide (114 mg, 1.00 mmol) was added to the frozen mixture. The reaction mixture was warmed up to −30 °C and mixed until a clear solution was obtained. In dynamic vacuum excess HF was removed at −78 °C. The compound was obtained as a colorless crystalline solid. The rector was left in an ethanol bath at −70 °C for crystallization of **5**.

Deposition Numbers 2178675 (for **1**), 2178678 (for **5**), and 2178670 (for fumaramide) contain the supplementary crystallographic data for this paper. These data are provided free of charge by the joint Cambridge Crystallographic Data Centre and Fachinformationszentrum Karlsruhe Access Structures service www.ccdc.cam.ac.uk/structures.

Conflict of Interest

The authors declare no conflict of interest.

Data Availability Statement

The data that support the findings of this study are available in the supplementary material of this article.

[1] A. Greenberg, C. M. Breneman, J. F. Liebman, *The Amide Linkage: Structural Significance in Chemistry, Biochemistry, and Materials Science*, Wiley, New York, NY, **200**.

[2] J. I. Mujika, J. M. Matxain, L. A. Eriksson, X. Lopez, *Chem. Eur. J.* **2006**, *12*, 7215.

[3] C. R. Kemnitz, M. J. Loewen, *J. Am. Chem. Soc.* **2007**, *129*, 2521.

[4] T. Schirmeister, C. Schmuck, P. R. Wich, *Beyer/Walter Organische Chemie*, Hirzel Verlag, Stuttgart, **2016**.

[5] G. Meng, J. Zhang, M. Szostak, *Chem. Rev.* **2021**, *121*, 12746.

[6] L. Pauling, *The Nature of the Chemical Bond*, Cornell University Press, New York, **1940**.

[7] a) L. Pauling, R. B. Corey, H. R. Branson, *Proc. Natl. Acad. Sci. USA* **1951**, *37*, 205; b) D. Eisenberg, *Proc. Natl. Acad. Sci. USA* **2003**, *100*, 11207.

[8] A. S. Edison, *Nat. Struct. Biol.* **2001**, *8*, 201.

[9] K. P. C. Vollhardt, N. E. Schore, *Organische Chemie*, Wiley-VCH, Weinheim, **2020**.

[10] H. Hart, L. E. Craine, D. J. Hart, C. M. Hadad, *Organische Chemie*, Wiley-VCH, Weinheim, **2007**.

[11] R. Szostak, J. Aubé, M. Szostak, *Chem. Commun.* **2015**, *51*, 6395.

[12] D. Zahn, *J. Phys. Chem. B* **2003**, *107*, 12303.

[13] S. J. Cho, C. Cui, J. Y. Lee, J. K. Park, S. B. Suh, J. Park, B. H. Kim, K. S. Kim, *J. Org. Chem.* **1997**, *62*, 4068.

[14] G. A. Olah, G. K. Prakash, J. Sommer, *Science* **1979**, *206*, 13.

[15] G. A. Jeffrey, J. R. Ruble, R. K. McMullan, D. J. DeFrees, J. S. Binkley, J. A. Pople, *Acta Crystallogr.* **1980**, *B36*, 2292.

[16] A. F. Holleman, E. Wiberg, N. Wiberg, G. Fischer, *Anorganische Chemie*, De Gruyter, Berlin, Boston, **2017**.

[17] J. Axhausen, C. Ritter, K. Lux, A. Kornath, *Z. Anorg. Allg. Chem.* **2013**, *639*, 65.

[18] a) M. Finze, E. Bernhardt, H. Willner, C. W. Lehmann, F. Aubke, *Inorg. Chem.* **2005**, *44*, 4206; b) D. Leitz, M. C. Bayer, Y. Morgenstern, F. Zischka, A. J. Kornath, *Chem. Eur. J.* **2018**, *24*, 15825.

[19] T. Soltner, N. R. Goetz, A. Kornath, *Eur. J. Inorg. Chem.* **2011**, 3076.

[20] M. S. G. Flett, *Spectrochim. Acta* **1962**, *18*, 1537.

[21] J. Weidlein, U. Müller, K. Dehnicke, *Schwingungsspektroskopie*, Thieme, Stuttgart, New York, **1988**.

[22] M. Azeem, M. Brownstein, R. J. Gillespie, *Can. J. Chem.* **1969**, *47*, 4159.

[23] K. Govindan, W.-Y. Lin, *Org. Lett.* **2021**, *23*, 1600.

[24] J. Axhausen, *Ludwig-Maximilians-Universität, Diss.*, Universitätsbibliothek der Ludwig-Maximilians-Universität, München, **2013**.

[25] Rigaku Oxford Diffraction, CrysAlisPro Software System, *Version 1.171.38.46*, Rigaku Corporation, Oxford, UK, **2015**.

[26] G. M. Sheldrick, *Acta Crystallogr.* **2015**, *A71*, 3.

[27] G. M. Sheldrick, *Acta Crystallogr.* **2015**, *C71*, 3.

[28] L. J. Farrugia, *J. Appl. Crystallogr.* **1999**, *32*, 837.

[29] A. L. Spek, *J. Appl. Crystallogr.* **2003**, *36*, 7.

[30] SCALE3 ABSPACK, *An Oxford Diffraction Program*, Oxford Diffraction Ltd, UK, **2005**.

[31] M. J. Frisch, G. W. Trucks, H. B. Schlegel, G. E. Scuseria, M. A. Robb, J. R. Cheeseman, G. Scalmani, V. Barone, B. Mennucci, G. A. Petersson, H. Nakatsuji, M. Caricato, X. Li, H. P. Hratchian, A. F. Izmaylov, J. Bloino, G. Zheng, J. L. Sonnenberg, M. Hada, M. Ehara, K. Toyota, R. Fukuda, J. Hasegawa, M. Ishida, T. Nakajima, Y. Honda, O. Kitao, H. Nakai, T. Vreven, J. A. Montgomery, Jr., J. E. Peralta, F. Ogliaro, M. Bearpark, J. J. Heyd, E. Brothers, K. N. Kudin, V. N. Staroverov, R. Kobayashi, J. Normand, K. Raghavachari, A. Rendell, J. C. Burant, S. S. Iyengar, J. Tomasi, M. Cossi, N. Rega, J. M. Millam, M. Klene, J. E. Knox, J. B. Cross, V. Bakken, C. Adamo, J. Jaramillo, R. Gomperts, R. E. Stratmann, O. Yazyev, A. J. Austin, R. Cammi, C. Pomelli, J. W. Ochterski, R. L. Martin, K. Morokuma, V. G. Zakrzewski, G. A. Voth, P. Salvador, J. J. Dannenberg, S. Dapprich, A. D. Daniels, O. Farkas, J. B. Foresman, J. V. Ortiz, J. Cioslowski, D. J. Fox, *Gaussian 09, Revision A.02*, Gaussian, Inc., Wallingford CT, **2009**.

[32] M. J. Frisch, G. W. Trucks, H. B. Schlegel, G. E. Scuseria, M. A. Robb, J. R. Cheeseman, G. Scalmani, V. Barone, G. A. Petersson, H. Nakatsuji, X. Li, M. Caricato, A. V. Marenich, J. Bloino, B. G. Janesko, R. Gomperts, B. Mennucci, H. P. Hratchian, J. V. Ortiz, A. F. Izmaylov, J. L. Sonnenberg, D. Williams-Young, F. Ding, F. Lipparini, F. Egidi, J. Goings, B. Peng, A. Petrone, T. Henderson, D. Ranasinghe, V. G. Zakrzewski, J. Gao, N. Rega, G. Zheng, W. Liang, M. Hada, M. Ehara, K. Toyota, R. Fukuda, J. Hasegawa, M. Ishida, T. Nakajima, Y. Honda, O. Kitao, H. Nakai, T. Vreven, K. Throssell, J. A. Montgomery, Jr., J. E. Peralta, F. Ogliaro, M. J. Bearpark, J. J. Heyd, E. N. Brothers, K. N. Kudin, V. N. Staroverov, T. A. Keith, R. Kobayashi, J. Normand, K. Raghavachari, A. P. Rendell, J. C. Burant, S. S. Iyengar, J. Tomasi, M. Cossi, J. M. Millam, M. Klene, C. Adamo, R. Cammi, J. W. Ochterski, R. L. Martin, K. Morokuma, O. Farkas, J. B. Foresman, D. J. Fox, *Gaussian 16, Revision A.03*, Gaussian, Inc., Wallingford CT, **2016**.

[33] R. Dennington, T. A. Keith, J. M. Millam, *GaussView, Version 6.0*, Semichem Inc., Shawnee Mission, **2016**.